Pure dephasing induced single-photon parametric down-conversion in a strongly coupled plasmon-exciton system

Ruben Pompe,[1] Matthias Hensen,[2] Matthew Otten,[3] Stephen K. Gray,[4] and Walter Pfeiffer[1]
[1]*Fakultät für Physik, Universität Bielefeld, Universitätsstraße 25, 33615 Bielefeld, Germany*
[2]*Institut für Physikalische und Theoretische Chemie, Universität Würzburg, Am Hubland, 97074 Würzburg, Germany*
[3]*HRL Laboratories, LLC, Malibu, California 90265, USA*
[4]*Center for Nanoscale Materials, Argonne National Laboratory, 9700 South Cass Avenue, Lemont, Illinois 60439, USA*

(Received 20 July 2022; revised 31 August 2023; accepted 1 September 2023; published 26 September 2023)

We propose highly efficient photon pair generation via down-conversion in a polaritonic cyclic three-level system formed via coupling an exciton and a localized plasmon polariton. Pure dephasing of the exciton enables optical transitions from the upper to lower polariton state via symmetry breaking and thus opens a pathway for the cascaded emission of two photons. The strength of this down-conversion pathway is determined by the coupling strength between exciton and plasmon polariton and the exciton dephasing rate. In the case of strong up to ultrastrong coupling and strong dephasing, this results in a nanoscopic $\chi^{(2)}$-system capable of few-photon down-conversion. A semiconductor quantum dot embedded in a gap plasmon, which supports strong coupling between plasmon and exciton, in combination with fast pure dephasing in the quantum dot exciton, allows one to reach conversion efficiencies down to the single-photon limit under experimentally achievable parameters at ambient conditions.

DOI: 10.1103/PhysRevB.108.115432

I. INTRODUCTION

Photon conversion via nonlinear optical processes is a cornerstone in photonics. In addition to the generation of coherent light at tunable wavelengths [1,2], it is key to generating nonclassical states of light [3,4] required for technologies such as high-precision interference measurements via squeezed light [5] or quantum encryption via entangled states [6]. Furthermore, nonlinear processes enable matter-mediated photon-photon interactions essential for optical information processing. Such nonlinearities provide ways to split and merge optical information channels or apply computational operations via optical switches. The use of nonlinear processes in optical crystals is a standard procedure for photon conversion [7]. Phase-matching engineering and field concentration in photonic waveguides allow compensating for their low nonlinear coefficients, thus increasing conversion efficiencies. These approaches work in the regime of many pump photons [8,9] with down-conversion efficiencies of on average one down-converted photon pair from $\approx 2.5 \times 10^5$ to 4×10^6 incoming photons considered to be high [10]. For applications in highly integrated optical circuits, such conversion efficiencies lead to high losses, which are detrimental to energy efficiency and make heat management necessary. Thus, optical nonlinearities occurring in the regime of a single or a few pump photons are of the utmost importance [11]. Schemes using single photons and single atoms in a cavity kept at ultralow temperatures reach the regime of single-photon nonlinearities [12]. Recently, room-temperature single-photon nonlinearity was demonstrated in an organic polymer coupled to a dielectric microcavity employing stimulated Bose condensation from excited excitons into a coherent polariton ground state [13]. Because of the size of the microcavity, this scheme still relies on a pumped exciton reservoir with several hundred excitons to achieve strong enough coupling between the cavity and the polymer.

Here we show that ultrastrong coupling (USC) of a single two-level system (TLS), i.e., a semiconductor quantum dot (QD) exciton, to a plasmon polariton, which acts as resonator, in combination with efficient pure dephasing of the TLS, realizes a cyclic three-level system. A cyclic three-level system is the simplest quantum system to represent a $\chi^{(2)}$ material, and it can, in principle, it can achive down-conversion efficiency of unity [14–16]. The proposed scheme opens up ways to both reduce the size of a nonlinear optical device and achieve single-photon nonlinearities without major pumping losses at ambient conditions. Here, we focus on a down-conversion process, efficiently converting an incident photon into a photon pair, both for degenerate and nondegenerate cases.

The manuscript is structured as follows: In Sec. II, the polaritonic Hamiltonian used for the subsequent considerations is introduced, as well as both the Lindblad master equation and the Redfield equation for the hybridized systems used to calculate the time evolutions. The section closes with an intuitive explanation of how the combination of TLS pure dephasing and strong coupling between the TLS and the plasmon polariton results in a cyclic three-level system, enabling efficient down-conversion of photons. In Sec. III, examples for physical realizations of strongly coupled exciton-plasmon systems are proposed, and we suggest a corresponding model system based on a semiconductor quantum-dot exciton coupled to a gap plasmon mode, with experimentally determined values reported in the literature as parameters for our simulations. We present the simulation results for degenerate

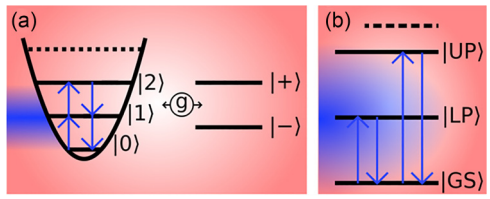

FIG. 1. Schematic representation of the polariton Hamiltonian. (a) Externally driven (blue shading) plasmonic mode coupled to an excitonic TLS is shown as separated subsystems. Both subsystems are embedded in bath systems (red background shading), which are responsible for dissipation of both subsystems. (b) The equivalent eigenstate basis representation as a polariton, with ground state (GS), lower polariton state (LP), and upper polariton state (UP). Higher-lying states are represented by horizontal black dashed lines. The blue arrows indicate the dipole allowed transitions (without pure dephasing).

down-conversion calculated via Lindblad and Redfield theories, as well an analysis of a heralded single-photon scheme calculated with Lindblad theory, which relies on nondegenerate down-conversion. The section closes with an estimation of the total device photon pair generation efficiency. The conclusion in Sec. IV summarizes the results and provides an outlook about possible applications of the proposed scheme.

II. THEORY

In this section, we first introduce the polaritonic Hamiltonian, which results from hybridization of the plasmon mode and the exciton, and its eigenbasis. Next, we briefly consider the Lindblad formalism that we use to handle the system-bath interaction. In particular, since we deal with a system of strongly interacting subsystems, the impact of this hybridization on external driving, output observables, and coupling to dissipative environments must be carefully considered. In this context, the effect of pure dephasing of the exciton on the hybridized system is presented. It is shown that this pure dephasing of a subsystem enables the otherwise forbidden transition between the upper and lower polariton state. While the Lindblad formalism is widely used due to its phenomenological nature and computational efficiency, we will also refer here to the Redfield formalism, which involves a more realistic physical model for the system-bath interaction and the pure dephasing of the system caused by it. By matching the results of both methods, we can justify the use of the phenomenological Lindblad approach and ensure that the pure dephasing effect necessary for the highly efficient down-conversion scheme proposed herein is not an artifact of the approximations made in the Lindblad approach. The section ends with an intuitive explanation of how pure dephasing of a subsystem in a hybrid system realizes a cyclic three-level system and thus enables efficient down-conversion.

A. Polariton in the ultrastrong coupling regime

The cavity quantum electrodynamics (cQED) Hamiltonian of a polariton resulting from the hybridization of a plasmonic mode and an excitonic TLS, as sketched in Fig. 1(a), reads [17]

$$H_{\mathrm{sys}} = \underbrace{\Omega_{\mathrm{m}}\, b^{\dagger} b}_{H_{\mathrm{m}}} + \underbrace{\Omega_{\mathrm{e}}\, \sigma_{+}\sigma_{-}}_{H_{\mathrm{e}}} + \underbrace{g\,(b^{\dagger}+b)(\sigma_{+}+\sigma_{-})}_{H_{\mathrm{int}}} + \underbrace{\frac{g^2}{\Omega_{\mathrm{e}}}(b^{\dagger}+b)^2}_{H_{\mathrm{dia}}} \tag{1}$$

where H_{m} and H_{e} are the plasmon and TLS Hamiltonians, respectively. b ($b^{\dagger}$) is the bosonic annihilation (creation) operator for the plasmonic mode, σ_{-} (σ_{+}) is the TLS lowering (raising) operator, and Ω_{m} and Ω_{e} are the boson mode and TLS level spacings, respectively. The coupling of plasmon and TLS with coupling strength g is described by the full dipole coupling Hamiltonian H_{int} and the energy contribution from the diamagnetic term H_{dia}, where the latter accounts for eigenenergy shifts which do not, however, affect the actual mechanism proposed here. Inclusion of counter-rotating and diamagnetic terms is necessary in the ultrastrong coupling regime, i.e., when $\eta = 2g/(\Omega_{\mathrm{m}} + \Omega_{\mathrm{e}}) \ll 1$ is not valid, since they significantly modify the energy spectrum [17]. The coupled system can be described in the diagonalized eigenbasis {GS, LP, UP, ...}, which assumes in the Bloch-Siegert regime, i.e., $\eta = 0.1$ and $\delta = |\Omega_m - \Omega_e| > 0$, the analytical expressions for the lowest three states relevant here [18]:

$$\begin{aligned}
|\mathrm{GS}\rangle &= \cos\left(\frac{\varphi_2}{2}\right)(|1,+\rangle + \lambda\sqrt{-1}|0,-\rangle) \\
&\quad + \sin\left(\frac{\varphi_2}{2}\right)(|2,-\rangle - \lambda\sqrt{n+1}|3,+\rangle) \\
|\mathrm{LP}\rangle &= \sin\left(\frac{\varphi_2}{2}\right)(|1,+\rangle + \lambda\sqrt{-1}|0,-\rangle) \\
&\quad - \cos\left(\frac{\varphi_2}{2}\right)(|2,-\rangle - \lambda\sqrt{n+1}|3,+\rangle) \\
|\mathrm{UP}\rangle &= \cos\left(\frac{\varphi_3}{2}\right)\left(|2,+\rangle + \lambda\sqrt{-1}|1,-\rangle\right) \\
&\quad + \sin\left(\frac{\varphi_2}{2}\right)(|3,-\rangle - \lambda\sqrt{n+1}|4,+\rangle)
\end{aligned} \tag{2}$$

with $\tan(\varphi_n) = 2g_n\sqrt{n}/\delta_n$, $\delta_n = \delta + 2n\omega_{\mathrm{BS}}$, $g_n = \sqrt{n}g - n^{\frac{3}{2}} g\,\omega_{\mathrm{BS}}/(\Omega_{\mathrm{m}} + \Omega_{\mathrm{e}})$, $\lambda = g/(\Omega_{\mathrm{m}} + \Omega_{\mathrm{e}})$, $\omega_{\mathrm{BS}} = \lambda^2$, and the product basis $|n, \pm\rangle$, where n represents the photon number (also known as Fock) state and + (–) denotes the excited (ground) state of the exciton.

B. Lindblad master equation for hybridized systems

The temporal evolution of the system's density matrix ρ_{sys} driven by an external classical light field, taking into account spontaneous dissipative transitions and pure dephasing in the framework of the Lindblad formalism [19], is described by the Liouville–von Neumann equation given by

$$\dot{\rho}_{\mathrm{sys}} = \frac{-i}{\hbar}[H_{\mathrm{sys}} + H_{\mathrm{dr}}, \rho_{\mathrm{sys}}] + \frac{1}{\hbar}\sum_i \Gamma_i\, L(o_i)[\rho_{\mathrm{sys}}] \tag{3}$$

with H_{sys} denoting the system Hamiltonian, H_{dr} modeling external driving, and the Lindblad terms $L(o_i)\,\rho = o_i\,\rho\,o_i^{\dagger} - (1/2)(\rho\,o_i^{\dagger}o_i + o_i^{\dagger}o_i\,\rho)$, where o_i is the jump operator for the ith system-bath interaction channel and Γ_i is the corresponding coupling energy. In the case of an uncoupled

boson and exciton, we consider three system-bath interaction channels., $i \in \{\mathrm{m}, \mathrm{e}, \varphi\}$. These are dissipation of the boson mode ($i = \mathrm{m}$) with strength Γ_m and jump operator $o_\mathrm{m} = b$, exciton dissipation ($i = \mathrm{e}$) with strength Γ_e and jump operator $o_\mathrm{e} = \sigma_-$ [both in Fig. 2(a), red arrows], and exciton pure dephasing ($i = \varphi$) with jump operator $o_\varphi = \sigma_+\sigma_-$ and rate Γ_φ [purple dashed shading in Fig. 2(a)]. For simplicity, pure dephasing of the boson mode, which for a plasmon could arise from electron-phonon interaction [20] or chemical damping [21], is neglected.

We consider that the plasmonic mode belongs to an efficient nanoantenna with a dominating coupling to the driving field and negligible direct driving of the TLS. For weak coupling g, such external driving is mediated by the bosonic field operator $b^\dagger + b$. However, at high coupling strength the plasmon and exciton hybridize and the driving term must be adapted, since the uncoupled driving field operator would directly act on exciton states due to the hybridization. H_dr is then given by [22]

$$H_\mathrm{dr} = \kappa\, f(t)(X_\mathrm{b}^\dagger + X_\mathrm{b}), \tag{4}$$

with $X_\mathrm{b} = \sum_{k,j>k} \langle j|b^\dagger + b|k\rangle |j\rangle\langle k|$ in the polariton eigenbasis $j, k \in \{\mathrm{GS}, \mathrm{LP}, \mathrm{UP}, \ldots\}$. $f(t)$ is a normalized real function reflecting the time-dependent driving, and κ is the effective coupling energy determined by the boson mode dipole moment and the maximum driving field. The same argument as for driving also holds for photon emission, and the emission spectrum $S(\omega)$ is then obtained as the real part of the Fourier transform of the adapted field correlator, i.e. [23],

$$S(\omega) = \Gamma_\mathrm{m}^{'}/\hbar \int_{-\infty}^{-\infty}\int_{-\infty}^{-\infty} \mathrm{Re}\left\{\left\langle X_\mathrm{b}^\dagger(t)\, X_\mathrm{b}(t+\tau)\right\rangle \exp(i\omega\tau)\right\} dt\, d\tau \tag{5}$$

where $\Gamma_\mathrm{m}^{'} = r_\mathrm{m}\Gamma_\mathrm{m}$ and r_m is the ratio between radiative loss ($\Gamma_\mathrm{m}^{'}$) and total loss (Γ_m) of the boson mode [24]. As for the case of the driving field, photon emission, i.e., the output field, is assumed to occur exclusively via the boson mode. Related quantities that require spectral selectivity, such as photon pair yields, heralding efficiency, etc., are calculated via transition-specific output observables (see Appendix A).

Treating bath interaction channels separately for each constituent also works only if the subsystems do not interact too strongly, i.e., $\eta \ll 1$. To obtain physically correct results, such as relaxation into the physical equilibrium state, in the strong and ultrastrong coupling regime modifications are again necessary due to hybridization of the subsystems. In this case, the full field and dipole coupling to the bath has to be considered for the dissipative jump operators for the subsystems, i.e., $o_\mathrm{m} = b^\dagger + b$ and $o_\mathrm{e} = \sigma_+ + \sigma_-$, since these Hermitian operators reflect the full physical coupling of the subsystems to their respective environments. Further, the jump operators of the coupled system $o_{jk} = |j\rangle\langle k|$ are expressed in the polariton eigenbasis, and the transition strengths Γ_{jk} are given by [25]

$$\Gamma_{jk} = \sum_i \Gamma_i(\Delta_{jk})|\langle j|o_i|k\rangle|^2 \tag{6}$$

for each $k \to j$ transition, where $k \geqslant j$ holds for transition energies much larger than the thermal energy of the bath.

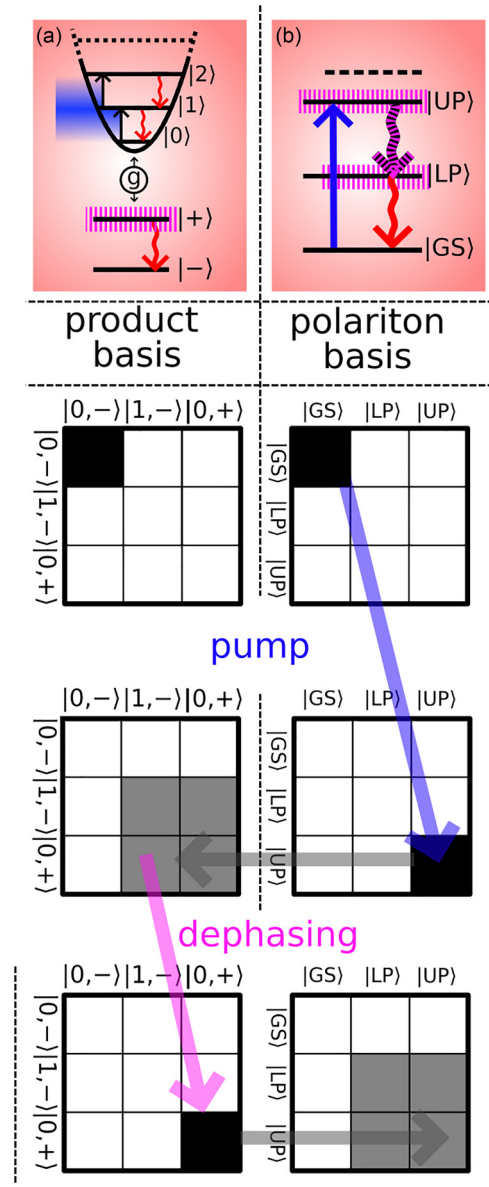

FIG. 2. Effect of exciton pure dephasing in a polariton state. (a) Level scheme including the possible transitions in the considered open polariton system in the product basis (upper). Resonant driving of the boson mode induces the LP to UP transition (blue arrow). Pure dephasing (purple shading) of the TLS is nondissipative in the uncoupled system. Below, a schematic of the density matrix in the uncoupled product basis. (b) Level scheme including possible transitions in the polariton eigenbasis. Resonant pump excites from GS to UP. Contrary to the uncoupled case, pure dephasing is dissipative in the polariton, causing LP to UP transitions. Dissipation of exciton and plasmon enables the LP to GS transition, closing the cycling three-level scheme. Below, a schematic of the density matrix in the polariton eigenbasis. First, the pump prepares the system in UP, an eigenstate of the polariton Hamiltonian. Next pure dephasing performs a measurement of the exciton state projecting the polariton into an eigenstate of o_φ, i.e., either $|0,+\rangle$ or $|1,-\rangle$ (here shown for $|0,+\rangle$), yielding LP population. The horizontal gray arrows indicate basis transforms between product state basis (a) and eigenstate basis (b) and vice versa.

Here the fact that $\Gamma_i(\Delta_{jk})$ is a function of the energy spacing $\Delta_{jk} = E_k - E_j$ between the relevant states is explicitly noted. In the proposed scheme, the relevant transitions between the polariton states are close to the level spacings of the uncoupled exciton and plasmon mode.

In the Lindblad treatment, it is implicitly assumed that the exciton pure dephasing couples to an excitation with a white noise spectrum, which is not the case for realistic scenarios in which, for example, pure dephasing is mediated by phonons. Thus, we investigate in Sec. II C the impact of a structured bath spectrum that provides small excitation energies using Redfield theory, where the exciton pure dephasing occurs via a strongly detuned coupling to low-energy phonon modes. This alternative modeling of the system-bath interaction will demonstrate that for the chosen excitonic systems, interactions with the environment can indeed be appropriately described by the Lindblad formalism, i.e., as a Markovian process, and resulting in stochastic, projective measurements of the open polariton system. For pure dephasing of excitons in QDs, this assumption does not hold in general and memory effects might significantly alter the system dynamics. However, in self-assembled semiconductor QDs, the pure dephasing process is in general non-Markovian due to retarded backaction of phonons scattered by the exciton [26]. Therefore, we restrict our considerations to specific kinds of QDs, such as colloidal QDs embedded in a suitable chemical, like ligands, or a mechanical environment, and thus we avoid considering non-Markovian quantum dynamics. This assumption does not imply that the proposed mechanism is absent for a non-Markovian dephasing mechanism, it is merely made to simplify the theoretical framework.

C. Redfield equation

The Lindblad master equation is an established framework to model the time evolution of open quantum systems, especially the treatment of system-bath interaction via phenomenological rate constants and jump operators. However, the Lindblad formalism implicitly assumes a flat spectrum of the bath correlations, i.e., the bath is randomly oscillating at all frequencies with the same amplitude, or in other words the noise power spectrum has a white spectrum. Since the phonon bath is responsible for the exciton pure dephasing process in actual physical realizations of our scheme proposed herein, the white noise environment assumed in the Lindblad formalism poses a conceptual problem. In principle, environmental noise resonant to the UP to LP transition could induce deexcitation instead of the proposed pure dephasing induced mechanism. To unambiguously identify the pure dephasing induced mechanism, it is thus essential to demonstrate that the cyclic three-level system responsible for efficient down-conversion occurs also for a more realistic system-environment interaction, which accounts for a realistic noise spectrum of a phonon bath.

To model a realistic phonon bath noise power spectrum, we employ here the Redfield theory approach [27]. Thus, calculations in Redfield theory are also presented in this manuscript, loosening the flat bath assumption, while keeping the remaining assumptions of the Lindblad formalism, i.e., the Born-Markov approximation. For the modeling we rely on the Redfield solver implemented in QuTiP, with the respective constraints on system-bath coupling operators [28]. It works with the density operator time evolution differential equation

$$\dot{\rho}_{ij}(t) = -i\frac{E(t)_{ij}}{\hbar}\rho_{ij}(t) + \sum_{k,l} R(t)_{ijkl}\rho_{kl}(t), \tag{7}$$

with $\{i, j, k, l\}$ indicating the whole system Hamiltonian eigenstates including the driving term, which are therefore time-dependent, $E(t)_{ij} = E(t)_i - E(t)_j$ is the energy difference between the eigenstates, ρ_{ij} are the density operator elements, and R_{ijkl} are the elements of the Redfield tensor. It is given by

$$R_{ijkl} = -\frac{1}{2}\sum_{\alpha}\left\{\begin{array}{l}\delta_{ij}\sum_n A^{\alpha}_{in}A^{\alpha}_{nk}J_{\alpha}(E_{kn}) - A^{\alpha}_{ik}A^{\alpha}_{lk}J_{\alpha}(E_{ki}) \\ +\delta_{ik}\sum_n A^{\alpha}_{ln}A^{\alpha}_{nj}J_{\alpha}(E_{ln}) - A^{\alpha}_{ik}A^{\alpha}_{lj}J_{\alpha}\big(E_{lj}\big)\end{array}\right\}. \tag{8}$$

δ_{ij} is the Kronecker delta, and $J_{\alpha}(E)$ is the noise-power spectrum of the environment labeled by α, coupled to the system by the Hermitian operator A^{α} [28]. The time dependency of R and the matrix elements of A^{α} are dropped to simplify the notation.

Plasmon mode and exciton resonance energies, as well as their coupling strength, are chosen identical to those used in the Lindblad calculations. Note that the system simulated by Redfield theory differs from the system simulated with the Lindblad master equation in two respects. First, the Redfield equation itself accounts for hybridization of the system, including the driving field, and second, the interaction with the phonon bath is modeled fundamentally differently. Hence a direct quantitative match cannot be the goal of the different models, and the comparison given here is first of all qualitative and serves to demonstrate that the proposed scheme for efficient down-conversion holds also under the assumption of a physically more realistic model for the phonon bath. Details of the calculations are given in Appendix C.

The phonon noise-power spectrum is taken to be of the standard form $J_{\varphi}(\omega) \sim \omega^3 \exp(-\frac{\omega^2}{\omega_c^2})$ [29], with a cutoff frequency ω_c, coupling to the exciton via $A^{\varphi} = \sigma_+ \sigma_-$. The bath of electromagnetic excitations leading to radiative damping of exciton and plasmon mode is represented with flat spectra, which vanish for negative energies, representing the EM vacuum. The spectral intensity is adapted to yield the same dissipation rates for both isolated subsystems as in the Lindblad simulations. The coupling with the bath is mediated by the Hermitian operators $A^{\mathrm{m}} = b^{\dagger} + b$ and $A^{\mathrm{e}} = \sigma_+ + \sigma_-$ for plasmon mode and exciton, respectively. These system-bath coupling operators are the same as for the Lindblad approach before correcting for the hybridization effect [Eq. (6)]. Note that in the Redfield approach, the hybridization effects are accounted for by propagating the density matrix in the combined eigenbasis of the unitary system Hamiltonian and the Hermitian system-bath coupling operators, including the time-dependent driving term. Still, as noted above, the modeling stays within the Markovian approximation, and memory effects in the phonon bath are neglected. However, since we also obtain the claimed emergence of a dephasing induced cyclic three-level system in a simplified quantum model

(Appendix D), which accounts for a coherent backaction of a phonon mode onto the polariton states, we assume that a non-Markovian bath will modify the efficiency of the proposed mechanism but not the dephasing induced down-conversion process itself.

D. Polaritonic cyclic three-level system via pure dephasing

Without pure dephasing of the TLS, the UP relaxes directly back into the GS only via the emission of a single fluorescence photon [Fig. 2(a)]. The cascaded emission of a photon pair is impossible since the transition matrix element for UP to LP vanishes, i.e., in Eq. (5) $\langle \mathrm{LP}|o_\mathrm{m}|\mathrm{UP}\rangle = \langle \mathrm{LP}|o_\mathrm{e}|\mathrm{UP}\rangle = 0$. In contrast, with pure dephasing, $\langle \mathrm{LP}|\mathrm{o}_\varphi|\mathrm{UP}\rangle \neq 0$ contributes to $\Gamma_{\mathrm{LP,UP}}$, i.e., UP $\rightarrow$ LP transitions and the emission of photons with energy $\Omega_{\mathrm{LP,UP}} = \Omega_{\mathrm{UP}} - \Omega_{\mathrm{LP}}$ become allowed [Fig. 2(b)]. When exclusively exciting UP, these transitions feed the LP population, and the emission of a second photon with energy $\Omega_{\mathrm{LP,GS}} = \Omega_{\mathrm{LP}} - \Omega_{\mathrm{GS}}$ ($\langle \mathrm{GS}|b^\dagger + b|\mathrm{LP}\rangle \neq 0$, $\langle \mathrm{GS}|\sigma_+ + \sigma_-|\mathrm{LP}\rangle \neq 0$) is a consequence of the initial UP $\rightarrow$ LP transition, yielding correlated photon pairs. This process closes the three-step transition cycle of absorbing one photon and emitting two down-converted photons [Fig. 2(a), left] serving as a basis for our proposed scheme of single-photon parametric down-conversion. The detuning between plasmon and exciton and the coupling strength g allow adjusting of the transition energies and thus enables choosing either degenerate or non-degenerate down-conversion. The strength of the UP $\rightarrow$ LP transition is determined by $\Gamma_{\mathrm{LP,UP}} = \Gamma_\varphi |\langle \mathrm{LP}|\mathrm{o}_\varphi|\mathrm{UP}\rangle|^2$ and depends on both the pure dephasing strength Γ_φ of the TLS and the coupling strength g. For $\Gamma_{\mathrm{LP,UP}} > \Gamma_{\mathrm{GS,UP}}$, relaxation under emission of two cascaded photons becomes dominant, and high down-conversion efficiencies are possible.

The finding that a pure dephasing mechanism opens new relaxation pathways for coupled systems can be rationalized based on the quantum trajectory formulation of system-bath interactions [19] [Fig. 2(b)]: The system is initially in the $|\mathrm{GS}\rangle$, which—neglecting virtual photons—is approximated by the product state $|\mathrm{m}, \mathrm{e}\rangle = |0, -\rangle$ (0 indicating no plasmon excitation and $-$ denoting the TLS ground state). The pump excitation induces a GS $\rightarrow$ UP transition via $\langle \mathrm{UP}|H_\mathrm{dr}|\mathrm{GS}\rangle \neq 0$. Resonant driving provides selectivity of the pump process, which is best understood in the polariton eigenbasis. In contrast, the pure dephasing mechanism acting on a subsystem is best conceived in the product state basis, where $|\mathrm{UP}\rangle$ is a coherent superposition of $|0, +\rangle$ and $|1, -\rangle$. The pure dephasing jump operator o_φ projects this superposition state either onto $|0, +\rangle$ or $|1, -\rangle$, i.e., an eigenstate of o_φ. However, both of these states are superposition states of $|\mathrm{UP}\rangle$ and $|\mathrm{LP}\rangle$ in the polariton eigenbasis. Hence, pure dephasing of a subsystem generates LP population and induces dissipation in the hybridized system causing emission of the first down-converted photon (Fig. 2). In conclusion, the UP $\rightarrow$ LP transition is the result of the projective measurement performed by the dephasing environment of the exciton. This mechanism is qualitatively different from the phonon-assisted transitions described elsewhere [30,31].

To check that the UP $\rightarrow$ LP transition relaxes via emission of a photon, and not into the phonon bath, we deployed a toy model with an explicitly modeled down-conversion resonant mode of the electromagnetic vacuum dipole-coupled to the polariton ($b^\dagger + b$), which is indeed populated. In addition, we modeled the phonon bath in Lindblad theory by coupling the exciton via o_φ to a single bosonic mode with an excitation energy in the meV range, i.e., far off-resonant to the exciton energy. In the time evolution of the expanded system, this phonon mode is populated. Destruction of a phonon or measurement of no phonon projects an also explicitly modeled EM mode resonant to the energy of the UP $\rightarrow$ LP transition into a state with significant probability for generating an instantaneous photon pair (see Appendix D).

III. SINGLE-PHOTON DOWN-CONVERSION IN A PLASMON – QUANTUM DOT POLARITON

A. Strong coupling between a quantum dot and a plasmon mode

The cyclic three-level down-conversion scheme discussed above (Sec. II D) is universal and can be realized for any kind of coupled quantum system with at least one constituent subject to pure dephasing. High coupling strength favors photon pair emission, and thus reaching the strong coupling (SC) limit or, ultimately, even the ultrastrong coupling regime (USC) is the second key ingredient for our proposed scheme. USC has been achieved in a variety of systems, such as in circuits of superconducting qubits [32], intersubband polaritons [33], Landau polaritons [34], plasmonic modes and organic molecules [35], optomechanical systems [36], and plasmonic resonances coupled to a Fabry-Pérot mode [37]. It is also possible to enhance the coupling strength by its square-root scaling when multiple emitters or modes are coupled together [38,39]. Note that also for such a multiemitter system, the scheme proposed herein works in the same way when the relevant subset of states can be approximated as TLS coupled to the plasmon mode. In addition to this many-emitter approach, strong spatial confinement of electromagnetic modes in plasmonic nanoresonators also allows for strong coupling even with single quantum emitters [40,41]. The latter two experimental demonstrations open a promising route towards the implementation of the scheme proposed herein, and as discussed in the following, the placement of a suitable colloidal semiconductor quantum dot in a gap plasmon represents a model system in which an efficient single-photon down-conversion process, as was discussed theoretically in Sec. II D, can be implemented.

Focusing on the goal to realize down-conversion functionality in the visible-infrared range in nanoscale devices, we explore the above-proposed scheme for a semiconductor QD exciton coupled to a tip-enhanced gap plasmon [40,41]. Nanostar nanoparticles on a metal mirror substrate with dielectric spacing layer provide ultra-small-mode volumes down to $V_\mathrm{m} = 1.05 \times 10^{-7}\lambda_\mathrm{m}^3$ ($\lambda_\mathrm{m} = hc/\Omega_\mathrm{m}$), and a high dissipation strength of $\Gamma_\mathrm{m} = 75$ meV, i.e., strong radiative damping. To account for nonradiative losses of the plasmon, we set $r_\mathrm{m} = 0.5$ [24], indicating that half of the energy is dissipated into internal Ohmic losses of the metal nanostructure. A semiconductor QD is used as TLS because its properties are widely tunable, e.g., by altering geometry or material doping. The used optical driving of the system is

optimized to inject, as close as possible, only a single photon. This avoids excitation of higher-lying energy states, and it both reduces the computational expenses by limiting the rank of the density matrix, and justifies the TLS approximation, i.e., that the excitation of biexciton states, which require the absorption of two photons, plays a negligible role.

As noted above, ultrafast dephasing for the TLS is desirable, and we assume the strongest pure dephasing strength reported in the literature of $\Gamma_\varphi = 94$ meV [42] between the exciton ground state and the excited state of PbSe QDs as the upper limit in the Lindblad simulation. For the Redfield simulations, a phonon bath spectrum with parameters for InGaAs QDs at a temperature of 295 K is used [43] (see Appendix C). We chose a high transition dipole moment $d = 140$ D, calculated with Fermi's golden rule [23] from a dissipation strength of $\Gamma_e = 0.66$ meV [44]. These parameters yield, based on the plasmonic field strength $\mathbf{E}$ and the TLS dipole moment d, the maximal coupling strength $g_{\max} = d|\mathbf{E}| = d\sqrt{\Omega_m/(2\varepsilon_0 V_m)} > 0.5\ \Omega_m$. We limit the following examples to cases of $g < 0.3\ \Omega_m$ to account for, e.g., nonperfect positioning. For all simulations, a transform-limited Gaussian excitation pulse with an intensity full width at half-maximum duration of 20 fs is used.

B. Degenerate down-conversion

The first example is the efficient generation of photon pairs with equal signal and idler photon energy $\Omega_s = \Omega_i = 1.55$ eV ($\lambda_{s(i)} = 800$ nm) from a $\Omega_p = 3.1$ eV ($\lambda_p = 400$ nm) pump photon. Depending on Γ_φ, pulsed excitation injects a mean total of $\langle N_{in}\rangle(\Gamma_\varphi = 0\ \text{meV}) = 0.97$ to $\langle N_{in}\rangle(\Gamma_\varphi = 94\ \text{meV}) = 0.77$ photons into the polariton (see Appendix B). As seen in Fig. 3(a), for low and moderate pure dephasing of the TLS, the direct pump photon fluorescence dominates. For stronger pure dephasing, the photon pair emission starts to dominate the emission spectrum $S(\Omega)$. As shown in Fig. 3(b), for pure dephasing strengths $\Gamma_\varphi > 40$ meV the photon pair yield per injected photon, defined as the number of photon pairs per pump photon, is $Y_{pair} > 0.5$. Losses are due to nonradiating deexcitations, UP $\rightarrow$ GS fluorescence, and, to a minor extent, spurious emission processes from excited states above UP (see Appendix C). The yield as a function of the dephasing strength exhibits a saturation behavior [solid line in Fig. 3(c)]. This is a direct consequence of the competing loss rates of the UP population. Because of the linear rise of Y_{pair} for weaker pure dephasing, even moderate pure dephasing yields already rather high down-conversion efficiencies before the saturation regime, limited by nonradiative losses, sets in.

The above-mentioned results are obtained using the Lindblad formalism, which assumes a white noise spectrum of the bath. Since the pure dephasing mechanism in QDs relies on the interaction of the TLS with phonons, the actual bath spectrum deviates strongly from a white spectrum. In particular, fluctuations in the bath correlation function oscillating at the UP $\rightarrow$ LP transition frequency might induce resonant dissipative transitions in the system and thus mimic the proposed down-conversion mechanism. To exclude such an artifact resulting from the basic assumptions of a flat spectrum in the Lindblad formalism, we employ in an example case Redfield theory, and we demonstrate that the efficient down-conversion proposed herein is reproduced in this case as well. Note that in Redfield theory, the system hybridization is treated differently. In particular, the driving field-induced effects on the system, i.e., the ac Stark shifts, are explicitly included. Consequently, the system parameters used in the Lindblad approach cannot be directly adopted for the Redfield case, and in addition the field strength should be kept small enough to exclude any impact due to ac Stark effects. The excitation pulse $f(t)$ [in Eq. (4)] is taken to be transform-limited with an intensity full

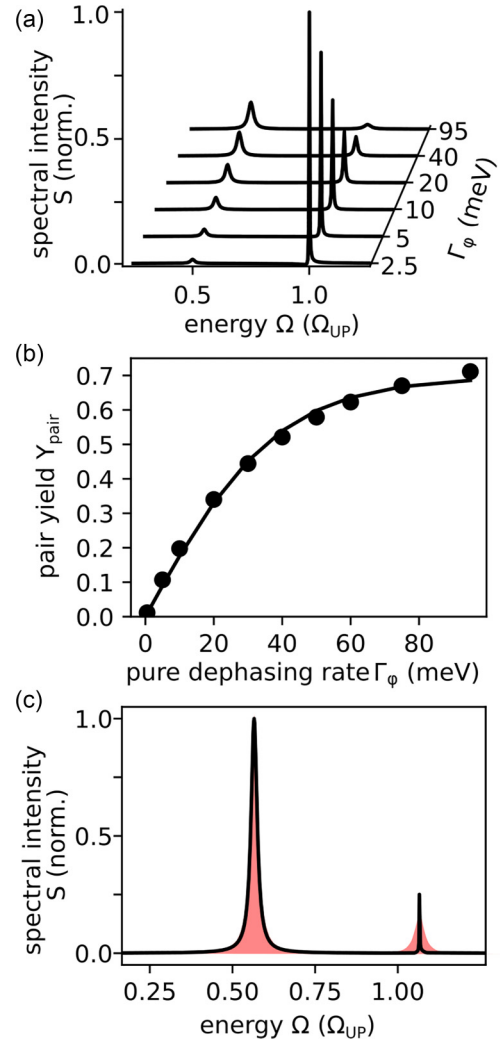

FIG. 3. Dephasing induced degenerate down-conversion in an ultrastrong coupled plasmon–quantum dot exciton hybrid. (a) Emission spectra of the degenerate configuration for varying QD pure dephasing strength Γ_φ, calculated with the Lindblad method. Spectra are normalized to the maximum of the series. (b) Calculated photon pair yield per injected photon (dots) with sigmoid fit (solid line). The plasmon resonance and exciton energy are $\Omega_m = 1.6$ eV ($\lambda_m = 775$ nm) and $\Omega_e = 2.9$ eV ($\lambda_e = 430$ nm), respectively. The relative coupling strength is $\eta = 0.233$ and the effective driving coupling is $\kappa = 260$ meV. (c) Emission spectrum of the degenerate configuration calculated via the Redfield method (normalized to the maximum). Note that the lower pump linewidth is due to the low weight of the structured phonon bath at this energy (for parameters see Appendix C; the Lindblad result for $\gamma_\varphi = 95$ meV is shown as a red shaded curve).

width at half-maximum (FWHM) of 20 fs and the maximum field strength is somewhat reduced compared to Lindblad calculations, resulting in an effective system-driving coupling $\kappa = 160$ meV and yielding on average $\langle N_{\text{in}} \rangle = 0.12$ of absorbed photons. All other simulation parameters are chosen so that the system dynamics match as closely as possible the case for $\Gamma_\varphi = 94$meV. As shown in Fig. 3(c), the emission spectrum matches closely the spectrum obtained based on the Lindblad formalism and as photon pair yield per injected photon $Y_{\text{pair}} \approx 0.45$ is obtained.

In the Redfield calculations, the UP $\rightarrow$ GS transition linewidth is much less broadened compared to the linewidth obtained in the Lindblad formalism. This is attributed to the much lower fluctuation amplitudes at high transition energies that are present in the Redfield approach and the thus much smaller linewidth broadening. However, again the UP $\rightarrow$ LP transition responsible for the cascaded two-photon emission is enabled by highly off-resonant coupling of this transition to phonon modes (cf. Appendix D), which leads to the efficient pure dephasing induced dissipation via this transition. Hence, the phonon-bath-induced probing of the polariton state via a projective measurement of the excited TLS state has the same impact within Redfield theory and in the Lindblad formalism. The reported down-conversion mechanism is thus not an artifact of the white noise spectrum assumed in the Lindblad formalism but is clearly reproduced using Redfield theory, which models the phonon bath more realistically. In the following, we will thus employ the much simpler Lindblad formalism.

C. Nondegenerate down-conversion

To demonstrate a nondegenerate process, we show a configuration that converts a pump photon at $\Omega_{\text{p}} = 1.94$ eV ($\lambda_{\text{p}} = 640$ nm) into a signal photon at $\Omega_{\text{s}} = 1.14$ eV ($\lambda_{\text{s}} = 1090$ nm) and an idler photon at $\Omega_{\text{i}} = 0.8$ eV ($\lambda_{\text{i}} = 1550$ nm). This is achieved by adjusting the detuning $\Omega_{\text{e}} - \Omega_{\text{m}}$ and the coupling strength g accordingly. The emission spectra [Fig. 4(a)] again reveal increasing down-conversion efficiency for increasing pure dephasing, i.e., the UP to GS fluorescence peak at Ω_{UP} shrinks as the pure dephasing is cranked up. For the given excitation, the average number of injected photons decrease from $\langle N_{\text{in}} \rangle(\Gamma_\varphi = 0 \text{ meV}) = 1.15$ to $\langle N_{\text{in}} \rangle(\Gamma_\varphi = 94 \text{ meV}) = 0.75$. An injected photon results on average in 0.57 signal photons and 0.34 idler photons for $\Gamma_\varphi = 94$ meV. The loss mechanisms are the same as for the degenerate case. The signal-idler photon pair yield per injected photon can again be approximated by a sigmoid function reaching $\text{Y}_{\text{pair}}(\Gamma_\varphi = 94 \text{ meV}) = 0.61$ [cf. Fig. 4(b)].

For such efficient down-conversion, the scheme becomes interesting as a heralded single-photon source. For $\Gamma_\varphi = 94$ meV, the detection of a signal photon heralds an idler photon with 91% confidence, and the detection of an idler photon gives 53% confidence for a signal photon [Fig. 4(b)]. The heralding capability of idler photons is rather independent of the dephasing, reflecting the fact that full LP population resulting from guaranteed idler emission inevitably leads to a LP $\rightarrow$ GS transition, radiating with assumed ~ 0.5 efficiency.

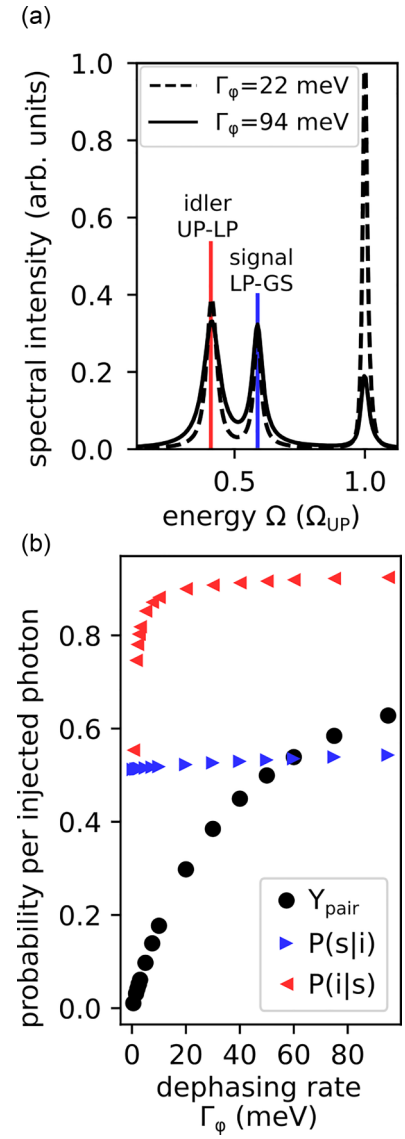

FIG. 4. Nondegenerate down-conversion process for application in a nanoscale heralded single photon source. (a) Emission spectra (normalized to the respective total emission) shown as a black solid line for $\Gamma_\varphi = 94$ meV, and a dashed line for $\Gamma_\varphi = 22$ meV calculated using the density matrix propagation based on the Lindblad formalism. (b) Pair yield per injected photon (circle), confidence that a signal photon heralds an idler photon (right pointing triangle), and probability that an idler photon heralds a signal photon (left pointing triangle) as a function of the TLS pure dephasing strength Γ_φ. The nanostar gap-plasmon resonance is at $\Omega_{\text{m}} = 1.4$ eV ($\lambda_{\text{m}} = 900$ nm) and coupled with a relative strength of $\eta = 0.275$ to a QD with an exciton energy of $\Omega_{\text{e}} = 1.62$ eV ($\lambda_{\text{e}} = 765$ nm). The effective driving coupling is $\kappa = 120$ meV.

D. Device output efficiency

The device output efficiency including coupling losses is estimated by calculating the input coupling efficiency ε as the ratio between the diffraction-limited spot size at the pump wavelength and experimental values for the extinction cross section of nanostars [45] with the respective resonance frequencies, resulting in $\varepsilon > 0.5$ for both the degenerate and

the nondegenerate case. We assume that the nanostar acts as an antenna, directing all extinguished light into a single mode with a sufficiently small mode volume. To account for deviations from these ideal cases, $\varepsilon = 0.1$ is used to calculate output efficiencies of one pair per 15 illuminating photons for the degenerate case at $\Gamma_\varphi = 94$ meV pure dephasing strength in the Lindblad calculation and also for the Redfield calculation, and 24 for the nondegenerate case for $\Gamma_\varphi = 94$ meV. This amounts in both cases to an increase in efficiency by four orders in magnitude in photon pair generation, compared to the highest reported experimental values [10].

IV. CONCLUSIONS

Based on cQED calculations, we propose an efficient single-photon down-conversion scheme, realizable with existing technology. In this scheme, the phonon bath of a QD exciton provides pure dephasing for one constituent of a coupled quantum system and thus induces the necessary symmetry breaking that enables a cascaded photon pair emission. For ultrastrong coupling between a plasmonic nanoresonator and a semiconductor QD subjected to strong pure dephasing, the pair production becomes the dominating relaxation pathway. This general scheme applies in any polaritonic system in which the UP-LP transition rate, enabled by the interplay of coupling and pure dephasing, is in the order of the UP-GS transition rate. Beyond ultrafast down-conversion, this scheme offers the means to decrease the impact of nonradiative losses and admits further nonlinear functionalities such as $\chi^{(3)}$ and $\chi^{(2)}$ photon up-conversion. Notably, the scheme works also for resonators with rather high quality factors such as dielectric microresonators [46] and small coupling g, as long as the pure dephasing mechanism is strong enough.

ACKNOWLEDGMENTS

This work was financially supported, in part, by the German Research Foundation (DFG) within the priority program SPP1839 Grant No. PF317-11/1 (Project No. 410519108). Work performed at the Center for Nanoscale Materials, a U.S. Department of Energy Office of Science User Facility, was supported by the U.S. DOE, Office of Basic Energy Sciences, under Contract No. DE-AC02-06CH11357.

APPENDIX A: CALCULATION OF FREQUENCY RESOLVED EMISSION PROPERTIES AND DERIVED QUANTITIES

To determine the expectation values of the radiated field resolved with respect to specific transitions, the individual Lindblad jump operators as defined in the main manuscript, i.e., the transition operators between the polariton eigenstates, are used for the construction of the relevant observables. For an individual transition, the output operator for the k to j transition O_{jk} reads

$$O_{jk} = \frac{\Gamma'_{jk}}{\hbar} |j\rangle\langle k|, \tag{A1}$$

with the output coupling strength corrected for nonradiative losses $\Gamma'_{jk} = r_{jk}\Gamma_{jk}$ as defined in the main manuscript. For the construction of an output field observable A_n for a particular detection channel n, a spectral filter is assumed, including only transitions with transition energies within the specific filter F_n. For simplicity, spectral overlap due to linewidths is neglected for the presented nondegenerate example. In general, the observables take the form

$$A_n = \sum\nolimits_{(j,k)\in F_n} O_{jk}. \tag{A2}$$

The yield of uncorrelated photons for a detection channel corresponding to a filter F_n is then given by

$$P_n = \int \langle A_n^\dagger(t) A_n(t)\rangle \, dt. \tag{A3}$$

The yield of correlated photon pairs is

$$\mathcal{G}^{(2)}_{nm} = \sum\nolimits_{(i,j)\in C_{nm}} \int\int \langle A_n^\dagger(t) A_m^\dagger(t+\tau) A_m(t+\tau) A(t)_n\rangle \, dt \, d\tau \tag{A4}$$

with $C_{nm} = \{(i, j)|i, j \in \{n, m\}\}$.

The probability that photons in channel F_n herald the detection of a photon in channel F_m is given by

$$\mathcal{H}^{(2)}_{nm} = \mathcal{G}^{(2)}_{nm} P_n^{-1}, \tag{A5}$$

where the factor P_n^{-1} normalizes the coincidence to a probability of 1 to detect a photon in channel n.

Due to the linearity of the trace and the linear relation between the radiative photon number operator for a specific set of transitions in F_n and their energy expectation values $\langle E_n\rangle$, the latter is given by

$$\langle E_n\rangle = \sum_{(j,k)\in F_n} (\Omega_k - \Omega_j)\langle O_{jk}^\dagger O_{jk}\rangle \tag{A6}$$

The total injected energy $\langle E_{\text{in}}\rangle$ is calculated by integrating over the temporal evolution of the expectation values for all dissipation channels. The pair yield per injected photon is then

$$Y_{\text{pair}} = \mathcal{G}^{(2)}_{nm} \, \Omega_{\text{pump}}/\langle E_{\text{in}}\rangle \tag{A7}$$

with the pump photon energy Ω_{pump}.

APPENDIX B: DEPHASING-DEPENDENT PHOTON INJECTION

For all simulations, all parameters are fixed except for the exciton pure dephasing strength Γ_φ, which is systematically varied to study its effect. In particular, the effective driving coupling constant κ and driving pulse shape are not varied. Accordingly, the total amount of injected energy varies with Γ_φ as shown in Fig. 5. This effect is attributed to the different dissipation rates and coherences of systems with different Γ_φ, while being identical in all other parameters. To estimate the deviation from linearity of the injection efficiency, the number of injected photons as a function of the dephasing strength is fitted with a power law,

$$f(\Gamma_\varphi) = a + b(\Gamma_\varphi)^c \tag{B1}$$

via the parameters a, b, and c. The fit parameters are $a = 9.7 \times 10^{-1} \pm 9 \times 10^{-4}$, $b = -7.05 \times 10^{-4} \pm 7.6 \times 10^{-5}$ meV^{-1}, $c = 1.25 \pm 3 \times 10^{-2}$ and $a = 1.159 \pm 2 \times 10^{-3}$, $b = -7.4 \times 10^{-3} \pm 6 \times 10^{-4}$ meV^{-1},

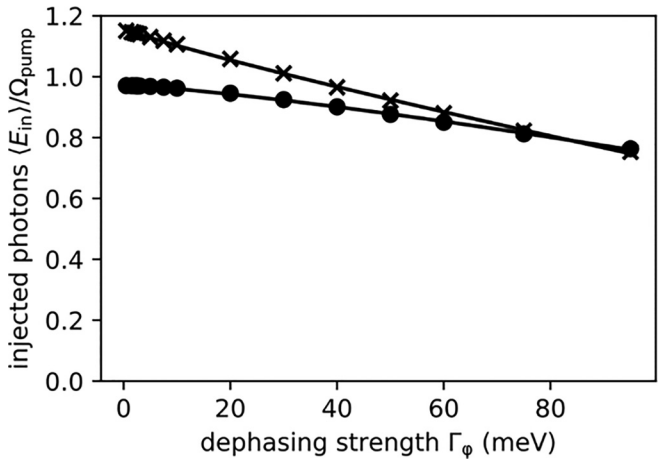

FIG. 5. Injected photons as a function of the exciton pure dephasing strength for the degenerate (crosses) and nondegenerate (circles) examples presented in the main manuscript. The curves represent the power-law fit.

$c = 8.8 \times 10^{-1} \pm 2 \times 10^{-2}$ for the degenerate and nondegenerate example, respectively.

The variation of the photon injection as a function of pure dephasing is significant but does not change the optical driving-induced system excitation too much. As mentioned in the main manuscript, this effect is taken into consideration by giving the relative yields, normalized to the total amount of injected energy, which varies with the strength of pure dephasing.

APPENDIX C: REDFIELD THEORY SIMULATIONS

The assumption of a flat noise-power spectrum as applied in the Lindblad master equation used for the calculations given in the main manuscript is rather strong. Hence to demonstrate that the down-conversion scheme described in the main manuscript is also possible when the applied model includes a physically motivated structured photon bath, the same polariton system time evolution was propagated with the expression for the time derivative given by Redfield theory, including a structured phonon noise-power spectrum $S(\omega)$ given by

$$J(\omega) = C\frac{\omega^3}{4\pi^2 D_m \hbar v^5}\left[d_e \exp\left(-\left(\frac{\omega a_e}{2v}\right)^2\right) - d_h \exp\left(-\left(\frac{\omega a_h}{2v}\right)^2\right)\right]^2, \tag{C1}$$

$$J_+(\omega) = J(\omega)\left(\frac{1+\exp\left(-c_T\frac{\omega}{T}\right)}{1-\exp\left(-c_T\frac{\omega}{T}\right)}\right),$$

$$J_- = -J(\omega)\left(\frac{\exp\left(-c_T\frac{\omega}{T}\right)}{1-\exp\left(-c_T\frac{\omega}{T}\right)}\right), \tag{C2}$$

$$S(\omega) = \begin{cases} J_+(\omega) & \text{if } \omega \geqslant 0, \\ J_-(\omega) & \text{if } \omega < 0, \end{cases} \tag{C3}$$

with C being a scaling constant, D_m is the lattice mass density, v is the speed of sound in the lattice, d_e and d_h are the electron and hole ground-state localization lengths, respectively, c_T is the constant for the temperature dependence, and T is the temperature. The resulting cutoff frequencies for electrons and holes are $\omega_{e,a} = \frac{a_e}{v} = 2.69$ THz and $\omega_{h,a} = \frac{a_h}{v} = 1.46$ THz. The numerical values are taken from [47] for GaAs quantum dots, and the temperature used for the calculation is $T = 295$ K (Fig. 6). The noise-power spectra for the electromagnetic vacuum as an environment for a quantum dot and a plasmon mode is flat.

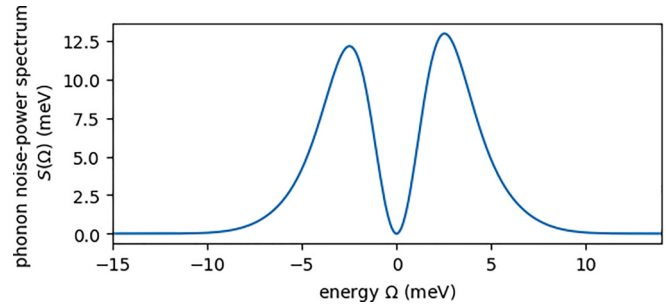

FIG. 6. Phonon noise-power spectrum. Calculated based on Eqs. (D1)–(D3) with $\Omega = \hbar\omega$ for parameters for GaAs quantum dots : $a_h = 1.9 \times 10^{-9}$ kg m^{-3}, $a_e = 3.5$ kg m^{-3}, $d_e = 7$, $d_h = -3.5$, $v = 5.11 \times 10^3$ m s^{-1}, $D_m = 5.37 \times 10^3$ kg m^{-3} at $T = 295$ K [47].

To maintain comparability of the Redfield calculations to the reference Lindblad master equation propagation, the strength of the external driving field is lowered compared to the value for the simulations described ($\kappa = 66$ meV) in the main manuscript, since the Redfield equation accounts for hybridization of the polariton and the driving field, influencing the eigenstates of the total system on which the environment acts. Weak driving minimizes the influence of this effect resulting from the differences in Lindblad and Redfield propagation.

As shown in Fig. 6, the phonon noise-power spectrum has most of its weight in the range of a few tenths of meV. The negative frequency peak is due to thermal pumping at ambient temperature, i.e., anti-Stokes interactions between the TLS and the phonon bath. The spectrum vanishes exponentially for higher values of ω because of the vanishing occupation of higher phonon number states. The minimum in the center reflects the diminishing phonon density of states for the acoustic branch. According to the mismatch between Ω_m and the noise spectrum frequencies, the phonon modes are coupled far off-resonance to the TLS representing the exciton in the quantum dot. While this condition prohibits real energy transfer from the TLS into the phonon bath, it still probes the state of a two-level system. Hence it is the transfer of quantum coherence from the TLS to the phonon bath without real energy transfer that enables the otherwise symmetry-forbidden transition from upper polariton state to lower polariton state.

The correlated photon pair yield is calculated from $\mathcal{G}^{(2)}$ in the same way as for the Lindblad simulations, but with a difference in the photon emission operators. Since for Redfield theory the dissipation and dephasing rate are not phenomenological parameters, they are not known *a priori*

to use them for input-output theory. Instead, the dissipation strength effectively resulting from the noise-power spectra into the electromagnetic vacuum is read out from the slope of population decays γ^{rf} in the numerical simulations. To account for nonradiative losses, the state overlap between the participating eigenstates of the polariton and the respective product states of plasmon mode and exciton is used to weight the different dark loss ratios $\eta_{\mathrm{plas(exc)}}$ reducing the effective number of photons emitted. The expressions for the emission strengths are

$$\Gamma^{\mathrm{rf}}_{\mathrm{LP,UP}} = \gamma^{\mathrm{rf}}_{\mathrm{LP,UP}} \left(\eta_{\mathrm{plas}} \sum_n |\langle \mathrm{UP}|n,0\rangle|^2 + \eta_{\mathrm{exc}} \sum_m |\langle \mathrm{UP}|0,m\rangle|^2 \right)$$
$$\Gamma^{\mathrm{rf}}_{\mathrm{GS,LP}} = \gamma^{\mathrm{rf}}_{\mathrm{GS,LP}} \left(\eta_{\mathrm{plas}} \sum_n |\langle \mathrm{LP}|n,0\rangle|^2 + \eta_{\mathrm{exc}} \sum_m |\langle \mathrm{LP}|0,m\rangle|^2 \right) \tag{C4}$$

The resulting dissipation operators used to calculate $\mathcal{G}^{(2)}$ are

$$A^{\mathrm{rf}}_{\mathrm{LP,UP}} = \frac{\Gamma^{\mathrm{rf}}_{\mathrm{LP,UP}}}{\hbar} |\mathrm{LP}\rangle\langle \mathrm{UP}|, \quad A^{\mathrm{rf}}_{\mathrm{GS,LP}} = \frac{\Gamma^{\mathrm{rf}}_{\mathrm{GS,LP}}}{\hbar} |\mathrm{GS}\rangle\langle \mathrm{LP}|. \tag{C5}$$

For the chosen driving scheme and noise-power spectrum of the phononic environment in the Redfield calculation, the normalized correlated photon-pair yield is $Y^{\mathrm{rf}}_{\mathrm{pair}} = 0.38$, compared to $Y_{\mathrm{pair}} = 0.31$ with the Lindblad master equation method.

APPENDIX D: IN-DEPTH DISCUSSION OF PHOTON DOWN-CONVERSION BY PHONON MEASUREMENT

To further illustrate how pure dephasing of the exciton can induce degenerate down-conversion resulting in the emission of a photon pair into a far-field mode coupled to the plasmon mode, we model the phonon bath, electromagnetic bath, and the interactions explicitly using a simplified Hamiltonian in which quantum coupling to the bath modes is reduced for each bath to a single mode. Pure dephasing of the exciton results from an interaction between exciton and phonon bath and thus is related to annihilation and creation of phonons. Explicit propagation of a suitably designed model system allows demonstrating that such a process indeed breaks symmetry and induces UP to LP transitions. To allow a straightforward propagation in time, both the phonon bath and the electromagnetic far-fields are represented by single bosonic modes with the corresponding energies of the quanta. This expanded model allows us to illustrate the UP state preparation by a measurement protocol, which is realized by the pure dephasing process. However, note that the down-conversion process shown in this appendix for single bath modes is the same for a continuum of such bath modes. The nonlinearity of quantum state measurements is exploited, for example, within the Knill-Laflamme-Milburn (KLM) protocol suggested for quantum computing in circuits with only linear operations besides measurements [48].

In the following, the extended model Hamiltonian [26]

$$\begin{aligned} H_{\mathrm{ext}} = & H_{\mathrm{sys}} + \Omega_{\mathrm{phon}} a^\dagger a + \gamma_\varphi \sigma_\varphi (a^\dagger + a) \\ & + \Omega_{\mathrm{phot}} c^\dagger c + \gamma_{\mathrm{m}} (b^\dagger + b)(c^\dagger + c) \end{aligned} \tag{D1}$$

is considered, with H_{sys}, γ_φ, γ_{m}, and σ_φ as defined in the main manuscript, as well as model parameters as used for the degenerate down-conversion Lindblad simulation (Sec. III B). $a^{(\dagger)}$, $b^{(\dagger)}$, and $c^{(\dagger)}$ are the bosonic annihilation (creation) operators of phonon, plasmon, and output photon modes, respectively. $\Omega_{\mathrm{phon}} = 25$ meV is the phonon energy, and $\Omega_{\mathrm{phot}} = 1.55$ eV is the electromagnetic far-field mode energy, resonant to the down-converted photon energy and coupled to the plasmon mode. The system is coupled to the respective baths via the Lindblad operators $\gamma_{\mathrm{m}}(r_{\mathrm{m}} - 1)L(c)$ for depopulation of the output mode, $\gamma_{\mathrm{m}} r_{\mathrm{m}} L(b)$ for Ohmic losses of the plasmon, $\gamma_\varphi n_{\mathrm{therm}} L(a^\dagger)$ for thermal pump by the bath of the phonon mode, and $\gamma_\varphi (n_{\mathrm{therm}} + 1) L(a)$ for its depopulation [19]. Ohmic losses and radiation from the TLS are neglected here for simplicity. The thermal phonon population is taken to be Bose-Einstein distributed, $n_{\mathrm{therm}} = (\exp(\frac{\Omega_{\mathrm{phon}}}{k_{\mathrm{B}} T}) - 1)^{-1} \approx 0.9$ at $k_{\mathrm{B}} T = 25$ meV. In contrast to the models without explicitly modeled bath modes (Secs. III B and III C), here the coherence of the TLS is lost by probing the phonon mode. This mode is coupled via $\sigma_\varphi (a^\dagger + a)$ to the TLS. The dephasing is now induced via detection of a phonon instead of applying σ_φ directly on the TLS, as it would result after tracing out the phonon mode. Note that the phonon mode is strongly off-resonant to the TLS or UP to LP transition. As shown below, this still enables an efficient UP to LP transition by phonon measurements. State measurement by dispersive coupled auxiliary systems is, e.g., an established method in circuit QED [49].

The system is initialized in the state ρ_0 with the polariton in the UP state and the rest of the system in the thermal equilibrium state ρ_{therm}. Hence ρ_0 can be expressed as

$$\rho_0 = |\mathrm{UP}\rangle\langle \mathrm{UP}| \otimes \mathrm{tr}_{\mathrm{pol}}\{\rho_{\mathrm{therm}}\}, \tag{D2}$$

with the second term on the right side representing the thermal state for which the polariton degrees of freedom are traced out.

To illustrate the process of state preparation by an individual projective measurement induced by the system interaction with the phonon bath mode, the effect of a phonon detection followed by the detection of a first down-converted photon at random times is calculated. Following such a single trajectory of a single quantum system reveals already the proposed mechanism of pure dephasing induced down-conversion. Accordingly, at a time t_1 the density matrix is transformed to

$$\rho(t_1) \to \frac{a\rho(t_1)a^\dagger}{\mathrm{tr}\{a\rho(t_1)a^\dagger\}}, \tag{D3}$$

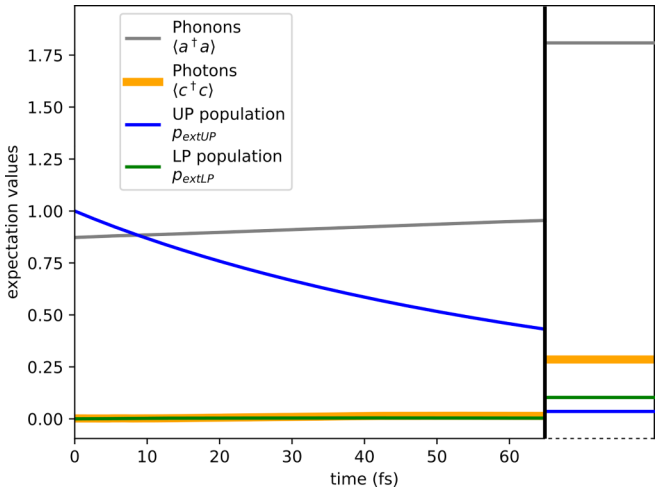

FIG. 7. Single quantum trajectory for state preparation by measurement of one phonon. Measurement of a phonon (black vertical line) results in a significant down-converted photon population in the output mode (orange). The right-hand lines represent the respective expectation values after the definite phonon measurement.

i.e., the system state after detection of a phonon, after left-side application of the phonon annihilator and right-side application of its Hermite conjugate on the density operator of the total system at time $t = t_1$.

Figure 7 summarizes the expectation values for phonons $\langle \sigma_+ \sigma_- \rangle$ (gray line), photons in the output mode $\langle c^\dagger c \rangle$ (orange), lower polariton state population $p_{\mathrm{LP}} = \langle |\mathrm{LP}\rangle\langle \mathrm{LP}| \rangle$ (green), and upper polariton state population $p_{\mathrm{UP}} = \langle |\mathrm{UP}\rangle\langle \mathrm{UP}| \rangle$ (blue) for an individual quantum trajectory. The initialization of the system with the polariton in the UP state and the output mode and the phonon bath in their thermal equilibrium states is a nonequilibrium state and starts to relax. Both dissipation of the plasmon mode into the far-field, which is not resonant to the down-converted photon energy, and Ohmic losses depopulate the UP state. In this process, the UP population decreases and the phonon number increases, since the exited polariton and thus TLS generates phonons. This relaxation of the UP state population continues until the phonon measurement occurs at $t_1 = 65$ fs. As expressed in Eq. (D3), the quantum state changes abruptly as a phonon is actually detected in the single-phonon mode that is explicitly modeled in the extended Hamiltonian H_{ext}. In this abrupt change, various things happen: First of all, and most interestingly in the context of the present work, the UP population drops to almost zero. This directly reflects the process, which enables the cyclic three-level scheme as discussed in Sec. II D, but now without relying on an approximate treatment of the TLS dephasing mechanism. In parallel to the reduction of the UP, both the LP population and the output mode photon occupation number expectation value exhibit an abrupt rise, i.e., a photon is indeed emitted as the UP to LP transition occurs. In addition, the phonon expectation value rises by about a factor 2. This reflects the thermal phonon bunching in the almost thermal state of the bosonic phonon mode, i.e., upon the detection of a first phonon there is a significantly higher probability to detect a second correlated phonon. Summarizing, this individual quantum trajectory of the extended Hamiltonian shows that the emergence of a cyclic three-level system indeed originates from the projective measurement that is phonon-induced by the pure dephasing of the TLS.

[1] G. Cerullo and S. De Silvestri, Ultrafast optical parametric amplifiers, Rev. Sci. Instrum. **74**, 1 (2003).

[2] R. W. Boyd, *Nonlinear Optics*, 4th ed. (Elsevier, Amsterdam, 2019).

[3] R. E. Slusher, L. W. Hollberg, B. Yurke, J. C. Mertz, and J. F. Valley, Observation of Squeezed States Generated by Four-Wave Mixing in an Optical Cavity, Phys. Rev. Lett. **55**, 2409 (1985).

[4] T. Basché, W. E. Moerner, M. Orrit, and H. Talon, Photon Antibunching in the Fluorescence of a Single Dye Molecule Trapped in a Solid, Phys. Rev. Lett. **69**, 1516 (1992).

[5] R. Schnabel, Squeezed states of light and their applications in laser interferometers, Phys. Rep. **684**, 1 (2017).

[6] C. Schimpf, M. Reindl, D. Huber, B. Lehner, S. F. Covre Da Silva, S. Manna, M. Vyvlecka, P. Walther, and A. Rastelli, Quantum cryptography with highly entangled photons from semiconductor quantum dots, Sci. Adv. **7**, eabe8905 (2021).

[7] C. J. Xin, J. Mishra, C. Chen, D. Zhu, A. Shams-Ansari, C. Langrock, N. Sinclair, F. N. C. Wong, M. M. Fejer, and M. Lončar, Spectrally separable photon-pair generation in dispersion engineered thin-film lithium niobate, Opt. Lett. **47**, 2830 (2022).

[8] H. Takesue, Single-photon frequency down-conversion experiment, Phys. Rev. A **82**, 013833 (2010).

[9] S. Zaske, A. Lenhard, and C. Becher, Efficient frequency down-conversion at the single photon level from the red spectral range to the telecommunications C-band, Opt. Express **19**, 12825 (2011).

[10] M. Bock, A. Lenhard, C. Chunnilall, and C. Becher, Highly efficient heralded single-photon source for telecom wavelengths based on a PPLN waveguide, Opt. Express **24**, 23992 (2016).

[11] D. E. Chang, V. Vuletić, and M. D. Lukin, Quantum nonlinear optics—photon by photon, Nat. Photon. **8**, 685 (2014).

[12] M. Brune, F. Schmidt-Kaler, A. Maali, J. Dreyer, E. Hagley, J. M. Raimond, and S. Haroche, Quantum Rabi Oscillation: A Direct Test of Field Quantization in a Cavity, Phys. Rev. Lett. **76**, 1800 (1996).

[13] A. V. Zasedatelev *et al.*, Single-photon nonlinearity at room temperature, Nature (London) **597**, 493 (2021).

[14] K. Koshino, Down-conversion of a single photon with unit efficiency, Phys. Rev. A **79**, 013804 (2009).

[15] E. Sánchez-Burillo, L. Martín-Moreno, J. J. García-Ripoll, and D. Zueco, Full two-photon down-conversion of a single photon, Phys. Rev. A **94**, 053814 (2016).

[16] P. Král and M. Shapiro, Cyclic Population Transfer in Quantum Systems with Broken Symmetry, Phys. Rev. Lett. **87**, 183002 (2001).

[17] A. Frisk Kockum, A. Miranowicz, S. De Liberato, S. Savasta, and F. Nori, Ultrastrong coupling between light and matter, Nat. Rev. Phys. **1**, 19 (2019).
[18] P. Forn-Díaz, G. Romero, C. J. P. M. Harmans, E. Solano, and J. E. Mooij, Broken selection rule in the quantum rabi model, Sci. Rep. **6**, 26720 (2016).
[19] H. J. Carmichael, *Statistical Methods in Quantum Optics 2: Non-Classical Fields* (Springer, Berlin, 2008).
[20] Z. Guo, B. F. Habenicht, W.-Z. Liang, and O. V. Prezhdo, *Ab initio* study of phonon-induced dephasing of plasmon excitations in silver quantum dots, Phys. Rev. B **81**, 125415 (2010).
[21] S. A. Lee and S. Link, Chemical interface damping of surface plasmon resonances, Acc. Chem. Res. **54**, 1950 (2021).
[22] A. Ridolfo, M. Leib, S. Savasta, and M. J. Hartmann, Photon Blockade in the Ultrastrong Coupling Regime, Phys. Rev. Lett. **109**, 193602 (2012).
[23] M. O. Scully and M. S. Zubairy, *Quantum Optics* (Cambridge University Press, Cambridge, 1997).
[24] S. Hughes, S. Franke, C. Gustin, M. Kamandar Dezfouli, A. Knorr, and M. Richter, Theory and limits of on-demand single-photon sources using plasmonic resonators: A quantized quasinormal mode approach, ACS Photon. **6**, 2168 (2019).
[25] F. Beaudoin, J. M. Gambetta, and A. Blais, Dissipation and ultrastrong coupling in circuit QED, Phys. Rev. A **84**, 043832 (2011).
[26] D. E. Reiter, T. Kuhn, and V. M. Axt, Distinctive characteristics of carrier-phonon interactions in optically driven semiconductor quantum dots, Adv. Phys.: X **4**, 1655478 (2019).
[27] A. G. Redfield, The theory of relaxation processes, in *Advances in Magnetic and Optical Resonance* (Elsevier, Amsterdam, 1965), Vol. 1, pp. 1–32.
[28] J. R. Johansson, P. D. Nation, and F. Nori, QuTiP 2: A Python framework for the dynamics of open quantum systems, Comput. Phys. Commun. **184**, 1234 (2013).
[29] T. Calarco, A. Datta, P. Fedichev, E. Pazy, and P. Zoller, Spin-based all-optical quantum computation with quantum dots: Understanding and suppressing decoherence, Phys. Rev. A **68**, 012310 (2003).
[30] F. J. P. Wijnen, J. H. Blokland, P. T. K. Chin, P. C. M. Christianen, and J. C. Maan, Competition between zero-phonon and phonon-assisted luminescence in colloidal CdSe quantum dots, Phys. Rev. B **78**, 235318 (2008).
[31] U. Hohenester, A. Laucht, M. Kaniber, N. Hauke, A. Neumann, A. Mohtashami, M. Seliger, M. Bichler, and J. J. Finley, Phonon-assisted transitions from quantum dot excitons to cavity photons, Phys. Rev. B **80**, 201311 (2009).
[32] F. Yoshihara, T. Fuse, Z. Ao, S. Ashhab, K. Kakuyanagi, S. Saito, T. Aoki, K. Koshino, and K. Semba, Inversion of Qubit Energy Levels in Qubit-Oscillator Circuits in the Deep-Strong-Coupling Regime, Phys. Rev. Lett. **120**, 183601 (2018).
[33] B. Askenazi, A. Vasanelli, Y. Todorov, E. Sakat, J.-J. Greffet, G. Beaudoin, I. Sagnes, and C. Sirtori, Midinfrared ultrastrong light–matter coupling for THz thermal emission, ACS Photon. **4**, 2550 (2017).
[34] A. Bayer, M. Pozimski, S. Schambeck, D. Schuh, R. Huber, D. Bougeard, and C. Lange, Terahertz light–matter interaction beyond unity coupling strength, Nano Lett. **17**, 6340 (2017).
[35] F. Barachati, J. Simon, Y. A. Getmanenko, S. Barlow, S. R. Marder, and S. Kéna-Cohen, Tunable third-harmonic generation from polaritons in the ultrastrong coupling regime, ACS Photon. **5**, 119 (2018).
[36] F. Benz *et al.*, Single-molecule optomechanics in "picocavities," Science **354**, 726 (2016).
[37] D. G. Baranov, B. Munkhbat, E. Zhukova, A. Bisht, A. Canales, B. Rousseaux, G. Johansson, T. J. Antosiewicz, and T. Shegai, Ultrastrong coupling between nanoparticle plasmons and cavity photons at ambient conditions, Nat. Commun. **11**, 2715 (2020).
[38] N. S. Mueller, Y. Okamura, B. G. M. Vieira, S. Juergensen, H. Lange, E. B. Barros, F. Schulz, and S. Reich, Deep strong light–matter coupling in plasmonic nanoparticle crystals, Nature (London) **583**, 780 (2020).
[39] T. Schwartz, J. A. Hutchison, C. Genet, and T. W. Ebbesen, Reversible Switching of Ultrastrong Light-Molecule Coupling, Phys. Rev. Lett. **106**, 196405 (2011).
[40] R. Chikkaraddy, B. de Nijs, F. Benz, S. J. Barrow, O. A. Scherman, E. Rosta, A. Demetriadou, P. Fox, O. Hess, and J. J. Baumberg, Single-molecule strong coupling at room temperature in plasmonic nanocavities, Nature (London) **535**, 127 (2016).
[41] H. Groß, J. M. Hamm, T. Tufarelli, O. Hess, and B. Hecht, Near-field strong coupling of single quantum dots, Sci. Adv. **4**, eaar4906 (2018).
[42] H. Kamisaka, S. V. Kilina, K. Yamashita, and O. V. Prezhdo, Ultrafast vibrationally-induced dephasing of electronic excitations in PbSe quantum dots, Nano Lett. **6**, 2295 (2006).
[43] A. Vagov, V. M. Axt, T. Kuhn, W. Langbein, P. Borri, and U. Woggon, Nonmonotonous temperature dependence of the initial decoherence in quantum dots, Phys. Rev. B **70**, 201305 (2004).
[44] J. C. Johnson, K. A. Gerth, Q. Song, J. E. Murphy, A. J. Nozik, and G. D. Scholes, Ultrafast exciton fine structure relaxation dynamics in lead chalcogenide nanocrystals, Nano Lett. **8**, 1374 (2008).
[45] *Gold Nanostars - Nanopartz*, https://www.nanopartz.com/bare-gold-nanostars.asp.
[46] S. Hu, M. Khater, R. Salas-Montiel, E. Kratschmer, S. Engelmann, W. M. J. Green, and S. M. Weiss, Experimental realization of deep-subwavelength confinement in dielectric optical resonators, Sci. Adv. **4**, eaat2355 (2018).
[47] A. Nazir, Photon statistics from a resonantly driven quantum dot, Phys. Rev. B **78**, 153309 (2008).
[48] E. Knill, R. Laflamme, and G. J. Milburn, A scheme for efficient quantum computation with linear optics, Nature (London) **409**, 46 (2001).
[49] G. Johansson, L. Tornberg, V. S. Shumeiko, and G. Wendin, Readout methods and devices for josephson-junction-based solid-state qubits, J. Phys.: Condens. Matter **18**, S901 (2006).